Medulla loss of scalp hair in breast cancer patients determined by near-infrared microscopy

Younshick Choi
Young-Ju Jeong
Jae-Geun Jeon
Sung-Hwan Park
Hye-Ryeon Choi
Jong-Ki Kim

SPIE.

Medulla loss of scalp hair in breast cancer patients determined by near-infrared microscopy

Younshick Choi,[a,†] **Young-Ju Jeong,**[b,†] **Jae-Geun Jeon,**[a] **Sung-Hwan Park,**[b] **Hye-Ryeon Choi,**[b] **and Jong-Ki Kim**[a,*]
aCatholic University of Daegu, School of Medicine, Biomedical Engineering, Daegu City, Republic of Korea
bCatholic University of Daegu, School of Medicine, General Surgery, Daegu City, Republic of Korea

Abstract. Inexpensive near-infrared microscopy (NIRM) was developed as a convenient technique to detect the medulla loss of scalp hair while reducing analytical time with easy sample preparation, leading to a field screening tool for breast cancer. NIRM has been evaluated as an alternative to synchrotron-based nanoscopy and to the relatively expensive method of conventional infrared microscopy to determine the degree and pattern of medulla loss of scalp hairs of patients with breast cancer and benign diseases, as well as normal healthy individuals. NIR imaging showed a strong, scattering-based hyperintense contrast of the medulla compared to the fully attenuated cortex in medullated healthy hair. Complete medulla loss (CML) per hair strand was more extensively ($60.9 \pm 10.2\%$) ($p < 0.001$) detected in the hair of all cancer patients than in the hair of either healthy individuals (less than $3.7 \pm 7.5\%$) or those with benign disease ($30.6 \pm 5.9\%$), suggesting a potential biomarker for breast cancer diagnosis. The medulla structure was retained mostly in the hair of age-matched healthy individuals, but discontinuous medulla loss was observed concomitantly with less CML in fibroadenoma patients. Potentially, compact NIRM modules can be integrated into a mobile platform as point-of-care technology for breast cancer screening. © The Authors. Published by SPIE under a Creative Commons Attribution 4.0 Unported License. Distribution or reproduction of this work in whole or in part requires full attribution of the original publication, including its DOI. [DOI: 10.1117/1.JBO.24.9.096501]

Keywords: near-infrared microscopy; hair; scattering; medulla; breast cancer screening; point-of-care technology.

Paper 190157R received May 15, 2019; accepted for publication Aug. 15, 2019; published online Sep. 11, 2019.

1 Introduction

New diagnostic methods that enhance the sensitivity and specificity of current screening modalities are necessary to identify women with early-stage diseases and to supplement the demonstrated role of mammography and breast ultrasound screening. As potent biomarkers for breast cancer diagnosis, various abnormal features of hair have been found in breast cancer patients, including the emergence of lipids detected by diffractometry[1,2] or FT-IR spectroscopy,[3] and medulla loss and cortical membrane enhancement, as observed by synchrotron x-ray nanoscopic imaging.[4] Since human hair grows at a rate of ∼2 cm per month, hairs of typical length retain a potent metabolic record associated with cancer initiation and growth. Therefore, measurements at a specific position in a hair strand (HS) retain morphological and metabolic features not only corresponding to the time of measurement but also temporally prior information. One may probe whole HSs with lengths of 10 cm, which would include diagnostic information over ∼5 months in an individual patient. Medulla loss in the hair structure has been previously detected by synchrotron x-ray nanoscopic imaging using zone-plate-based phase contrast but analyzed a limited length of HS for each measurement, less than 1 mm. In this regard, a faster, cheaper, and more convenient imaging method for detecting medulla loss in hair samples is required in practical clinical settings, such as point-of-care technology (POCT). In general, coarser hairs of adults are known to contain either discontinuous or continuous medulla,[5,6] but only a few studies,[4,7] including our prior work,[4] reported any transformation of the medulla

structure due to disease. The porous medulla structure was previously known to affect the appearance of hair color due to optical scattering by air in the pores[8,9] or to mechanical properties.[10] An advantage of NIR microscopy (NIRM) is the penetration of NIR light into the medulla and resulting interactions, such as light scattering with porous medulla structures, which may produce a unique contrast between the cortical matrix and medulla. In this study, a simple and cheap NIRM instrument was developed to image the internal structure of hair in order to detect differential alterations in medulla loss in optically opaque human scalp hair from breast cancer patients and age-matched healthy subjects. Herein, we present scattering-based medulla contrast in NIRM, which showed a distinctive pattern of loss as a molecular marker found in breast cancer patients. Since NIR microscopy can be integrated into a compact imaging or mobile POCT device, this finding may provide a convenient tool for breast cancer screening.

2 Materials and Methods

2.1 Hair Samples

Scalp hair samples from 20 breast cancer patients, five benign patients (four fibroadenoma and one phyllodes tumor), and seven breast cancer-negative healthy female volunteers were collected after obtaining informed consent at the Catholic University Hospital of Daegu in accordance with ethical standards for clinical trials (approval IRB CR-19-017-L). A total of 8 to 10 hair samples were collected from each patient. The cancer stage and histology at the time of sample collection are summarized in Table 1. The subjects ranged in age from 45 to 78 years, and the normal healthy group was age-matched with the breast cancer patients. All hair samples were collected

---

*Address all correspondence to Jong-Ki Kim, E-mail: jkkim@cu.ac.kr

†Both authors contributed equally.

Table 1 Summary of patient data.

Patient	Age	Histology and stage		CML	(Avg% ± SD)[a]
P1	45	Rt.IDC	T1bN0M0 stage IA	73.3	±43.4
P2	53	Rt.IDC	T1bN0M0 stage IA	73.3	±36.5
P3	47	Lt.IDC	T1bN0M0 stage IIA	60.0	±43.4
P4	—	Fibroadenoma	Benign	33.3	0.0
P5	54	DCIS		60.0	±43.4
P6	47	Lt.DCIS		66.7	±23.6
P7	30	Fibroadenoma	Benign	33.2	±23.5
P8	58	DCIS		73.3	±43.4
P9	53	DCIS		66.7	±47.1
P10	48	Phyllodes tumor	Benign	33.3	0.0
P11	37	IDC	T1bN0M0 stage IA	66.7	±23.6
P12	58	IDC	T1bN0M0 stage IA	73.3	±36.5
P13	59	IDC	T1aN0M0 stage IA	53.3	±50.5
P14	53	IDC	T1cN0M0 stage IA	46.7	±38.0
P15	78	DCIS		60.0	±43.4
P16	42	Lt.breast papillary Ca		60.0	±23.5
P17	45	Lt.IDC	T1bN0M0 stage IIIA	66.7	±23.6
P18	56	Rt.IDC	T1bN0M0 stage IIA	73.3	±36.5
P19	42	Lt.IDC	T1bN0M0 stage IA	43.4	±36.5
P20	46	Fibroadenoma	Benign	19.9	±18.2
P21	49	Rt.DCIS		66.7	±36.5
P22	49	Lt B fibroadenoma and sclerosing adenosis	Benign	33.3	±23.5
P23	52	Rt.IDC	T1bN0M0 stage IA	66.7	±23.6
P24	55	Lt. DCIS		60.0	±43.4
P25	43	Rt.IDC	T1bN0M0 stage IA	43.7	±33.4
P26	25	Negative		0.0	0.0
P27	30	Negative		0.0	0.0
P28	40	Negative		0.0	0.0
P29	50	Negative		13.3	±18.2
P30	51	Negative		0.0	0.0
P31	53	Negative		0.0	0.0
P32	63	Negative		0.0	0.0
P33	66	Negative		0.0	0.0
P34	68	Negative		0.0	0.0
P35	79	Negative		19.9	±13.6

[a]Average amount of CML per HS in a patient was estimated from five examined hairs and displayed as average% value ± SD.

from patients prior to any medical treatment including surgery or chemotherapy as reported previously.[4] All hair samples were cut close to the scalp from the bottom layer of hair on the nape of the scalp and were typically 5 to 9 cm in length.

2.2 NIR Microscopy Setup and Image Acquisition

All collected hair samples were divided equally into three sections from the root to the tip, and 15 to 20 mm of each section was examined on the scanned imaging. Two-dimensional (2-D) projection imaging of the hair samples was carried out using a homemade NIRM as shown in Fig. 1.

The intensity of the NIR LED at 860 nm was optimized to produce the best contrast of the medulla by controlling the power voltage and focusing with a combined objective lens and eyepiece. The optical axis could be shifted with the pitch and yaw stages. The sample was placed in the focus using the linear stage of the sample holder and further adjusted by moving the XY stage that was set perpendicular to the optical axis.

The focal length of the objective lens was 10 mm and was pretreated with B-coating (650 to 1050 nm) to maximize light transmission. An eyepiece (focal length: 12.5 mm) was attached to the detector using a CS-mount lens. A CMOS camera (Moticam X, Moticam, Hongkong) was used as a detector with a pixel size of 4.8 μm. The linear stage was set to the Z and X axes for alignment and focusing. Optical alignment of the NIRM system was performed by a red laser with height control.

For imaging with variable angle of incidence (AOI), the sample holder was set above the center of rotation stage pointing to the z axis. An LED light source was placed on the end of the rod, which was fastened on the rotation stage, as shown in Fig. 1. Images were acquired by changing the AOI of the light source from −20 deg to +30 deg using a built-in software (Motic Image Plus). NIR images acquired at AOI of 0 deg were stored at CMOS camera. We also tried to send NIR image of HS via Bluetooth to a smartphone where images can be processed further for diagnostic decision as shown in Fig. 1. This is presently under development in our lab. Each HS sample was divided into three segments with a size of 1.5 to 2 cm (tip side, middle, and root side) and imaged consecutively for each segment. Dominant pattern of medulla loss in each segment was categorized by three different patterns: complete medulla loss (CML), discontinuous medulla loss (DML), continuous (no loss).

The amount of CML observations among five examined hair samples and extension of CML per HS was measured from each cancer patient and compared to that of benign patients and healthy individuals.
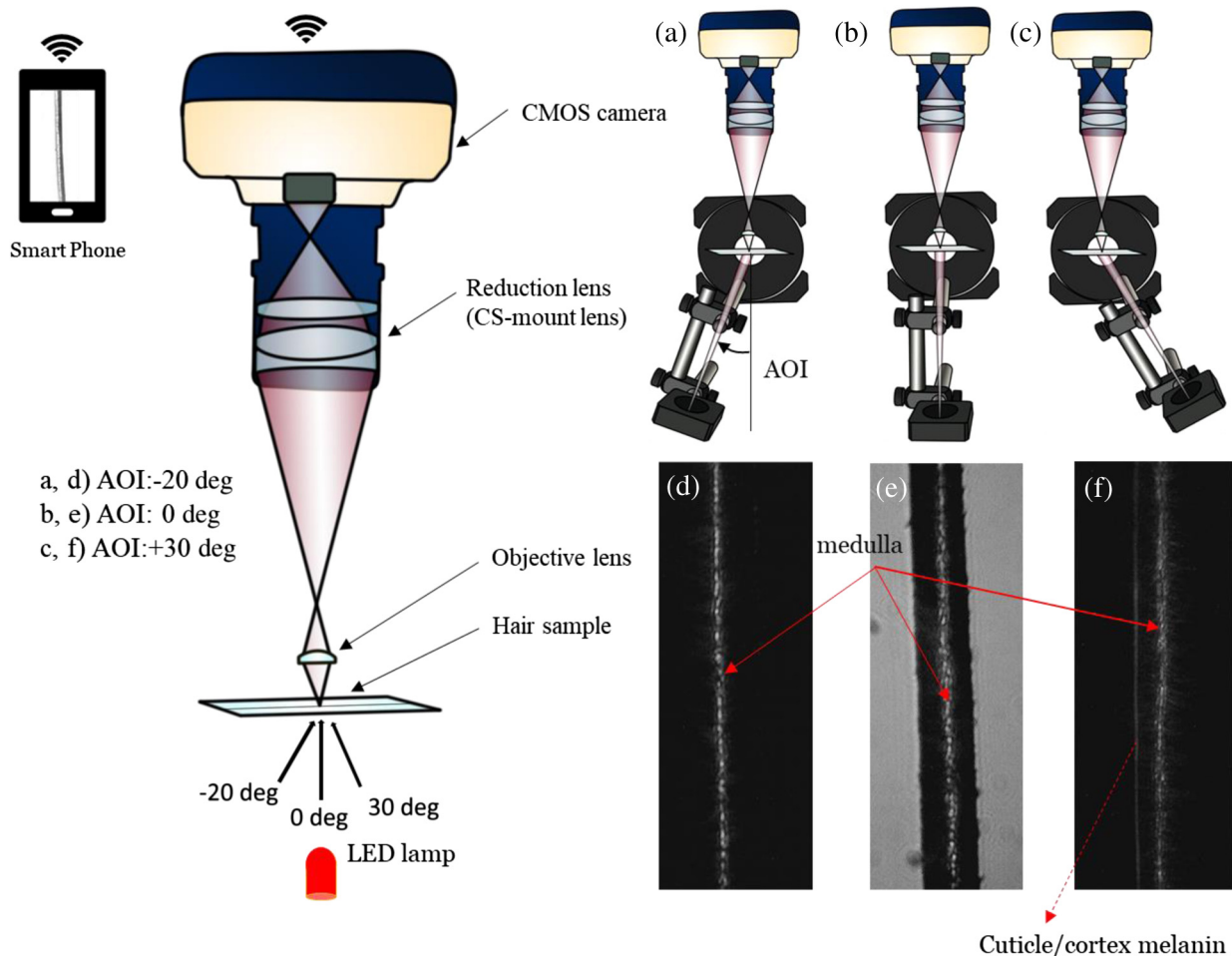

Fig. 1 Schematic diagram of NIR imaging set up for an HS (left side). Imaging of a medullated, healthy HS depending on the AOI (right side): (a), (d) AOI=−20 deg; (b), (e) 0 deg; and (c), (f) +30 deg. Porous medulla produced hyperintense scattering contrast (d)–(f), compared to attenuated cortex in NIR image with 860 nm.

2.3 IR Microscopy

2-D projection imaging of some hair samples was carried out using conventional IR microscopy (Nicolet iNIOMX, Thermo Fisher Scientific, Massachusetts) to compare with the NIRM images.

2.4 Synchrotron X-Ray Nanoscopy

Nanoscopic projection and CT scanning of the healthy hair samples were carried out using a monochromatic synchrotron x-ray (6.78 keV) at the Pohang Accelerator Laboratory (PAL) 7C beam line as described previously.[4,11] Reconstruction images of tomography data were obtained by applying a filtered backprojection algorithm to the projection image using the OCTOPUS software package (Ghent University, Belgium).[4]
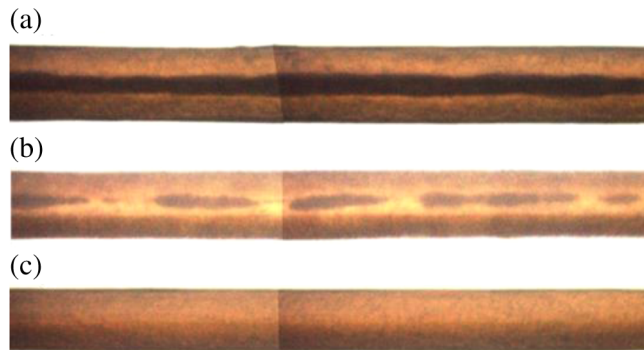
(a)

(b)

(c)

Fig. 2 IR imaging of HSs from a healthy individual (a) and patients with fibroadenoma (b) and breast cancer (c), demonstrating extensive medulla loss in the HSs of patients with cancer.

2.5 Statistical Analysis

The amounts of CML are presented as the mean ± standard deviation (SD) in Table 1. One-way analysis of variance (ANOVA) was used for data analyses. Levene's test was used to demonstrate equal variances of the variables. Post-hoc analysis using Bonferroni's multiple comparison test was used to determine significant differences by $p < 0.05$. All testing was performed using IBM SPSS statistical software v23 (IBM Corp., Armonk, New York).

3 Results and Discussion

Although conventional light microscopy does not reveal the medulla due to the optical opacity of black-colored hair, the medulla structure can be visualized by compound microscopy[8] or polarized light microscopy.[12] The medulla of a healthy HS contrasts well with the cortex on both NIR (Fig. 1) and IR imaging (Fig. 2).

In conventional IR microscopy, the medulla was revealed as a black strip band, indicating more attenuation compared to that in the cortex. In NIR imaging, contrast was reversed, as shown in Fig. 1. The medulla was shown to be hyperintense, and the cortex was hypointense. Moreover, the medulla was shown to be a rather speckled-like feature, suggesting the results of NIR scattering with some internal structure in the medulla.[8] The wavelength of NIR from the LED source was 860 nm, and it was not transmitted completely across the cortex in the whole diameter of healthy HS and appeared contrasted based on different optical properties between the cortex and medulla, as shown in Fig. 1(e).

Because the absorption coefficient of keratin, the major protein composing the cortex, is very low at wavelengths above
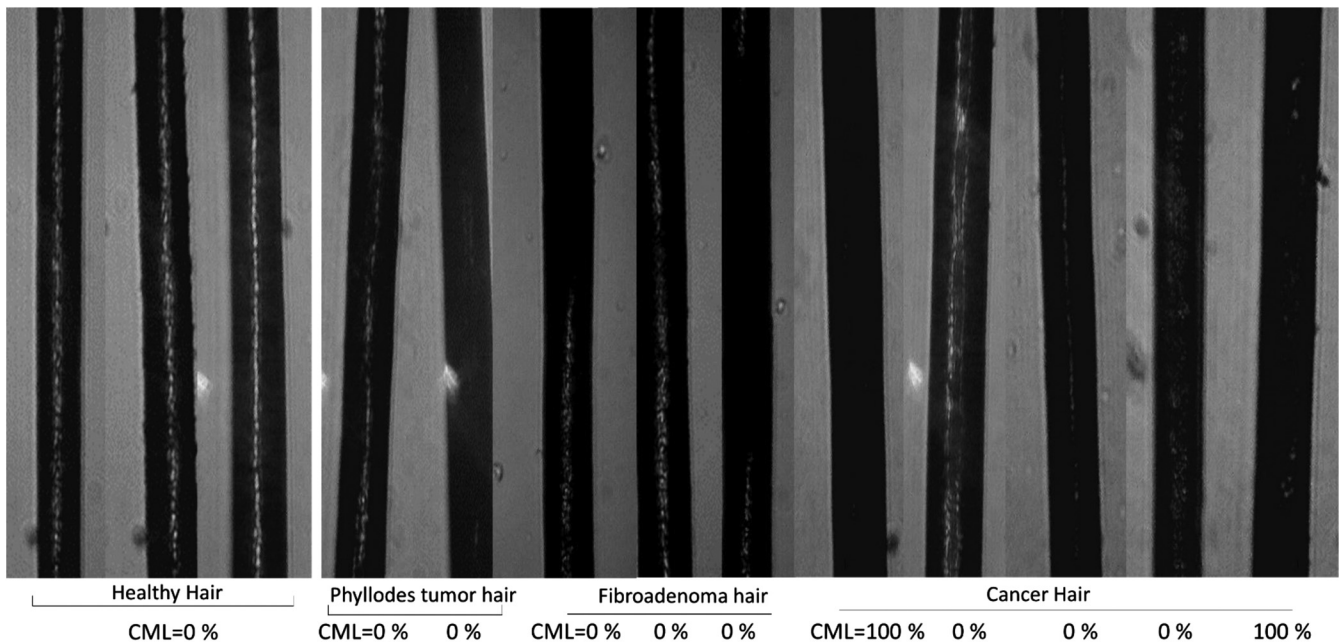

Healthy Hair	Phyllodes tumor hair		Fibroadenoma hair			Cancer Hair				
CML=0 %	CML=0 %	0 %	CML=0 %	0 %	0 %	CML=100 %	0 %	0 %	0 %	100 %

Fig. 3 Typical structural pattern of the HS part (FOV ∼ 1 mm) from healthy individuals, benign, and breast cancer patients. Continuous medulla distribution observed in healthy hair was modified into extensive loss (CML and mixture of CML and discontinuous loss) with various distribution patterns in cancer hairs while showing a discontinuous pattern of medulla loss in benign hairs (phyllodes tumor and fibroadenoma). CML was defined as a dominant pattern in an examined segment (1.5 to 2 cm HS) when medulla was absent continuously within more than 90% of the examined unit. Each CML number here demonstrated the value for whole 20 images of one segment, not presenting for the single view of 20 images.

400 nm, the total attenuation coefficient is dominated by the scattering coefficient. The total attenuation coefficient of a typical Asian black hair was close to 0.1 mm (similar scale of diameter of HS) around the NIR wavelength,[13,14] and bright-field imaging of a medulla-absent hair from a patient with cancer with forward incidence of light (0-deg AOI) showed complete

attenuation in the transmission-type NIRM at a wavelength of 860 nm, as shown in Fig. 3.

In contrast, we found AOI-dependent contrast between the cortex and medulla, as shown in Fig. 1. At a certain AOI (dark field mode), only a hyperintense scattering signal originating from the medulla structure was detected. The results suggested
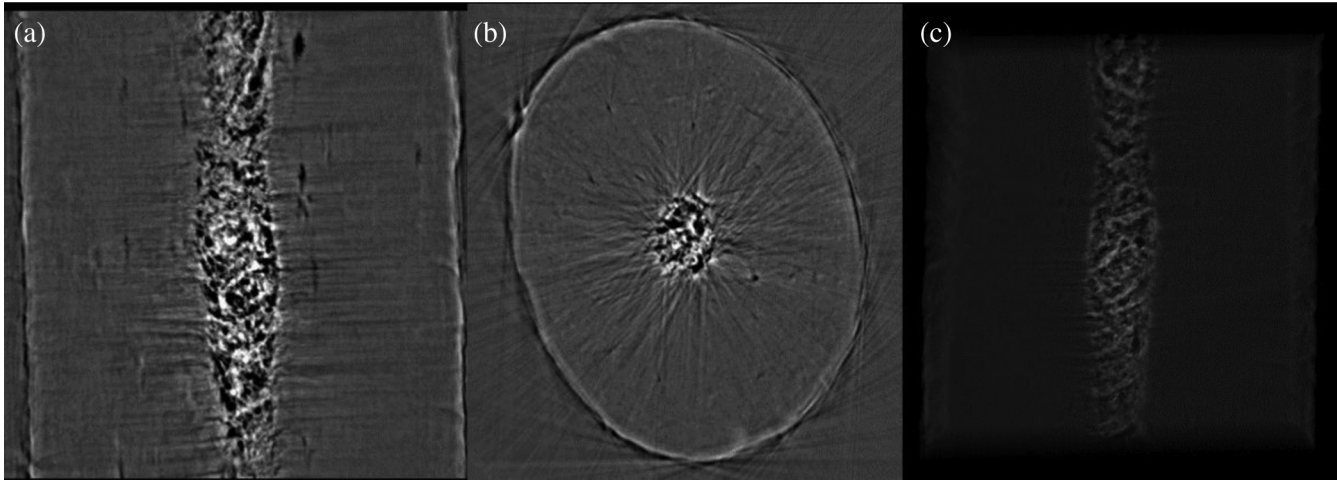

Fig. 4 Image of a healthy HS by synchrotron x-ray nanotomography showing a speckled-like medulla structure. Reformatted 2-D image in (a) a sagittal plane and (b) an axial plane. (c) A 3-D image of HS containing medulla.
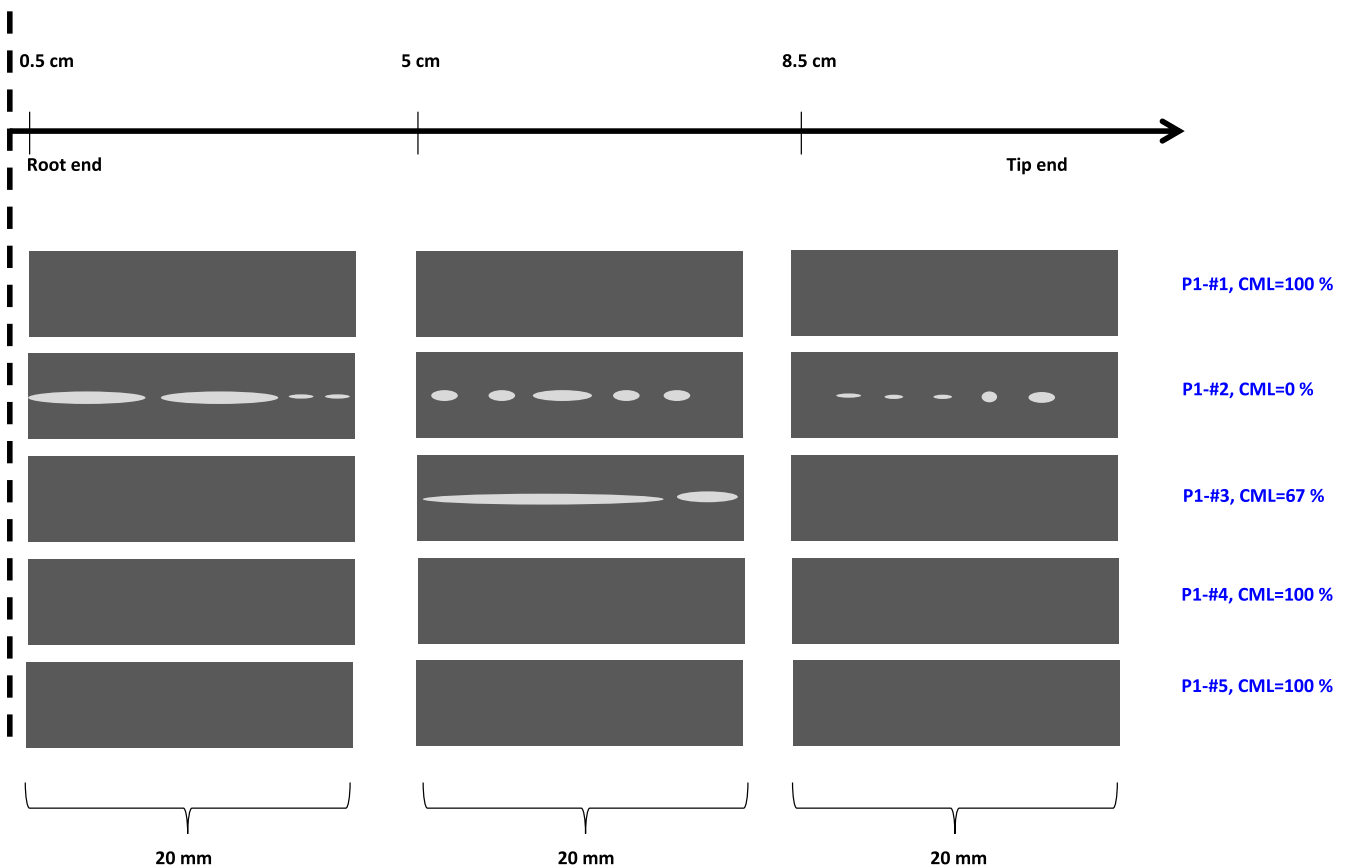

Fig. 5 Schematic diagram of typical medulla loss patterns in hair from a single cancer patient. Average CML was estimated 73% as indicated at P1 in Table 1. In the case of #2, DML was shown in complete HS, and #3 demonstrated DML only in the middle section of HS.

relatively strong scattering of NIR light with porous-like structures (a series of vacuoles) from the medulla that were also revealed more clearly on SR nanotomography, as shown in Fig. 4, or in a previous SEM imaging study.[15]

Therefore, the contrast we obtained in bright-field imaging, as shown in Fig. 1, originated due to strong scattering from the medulla and total attenuation across the cortex. The diameter of keratin fiber bundles in the hair cortex is much less than 0.1 μm,
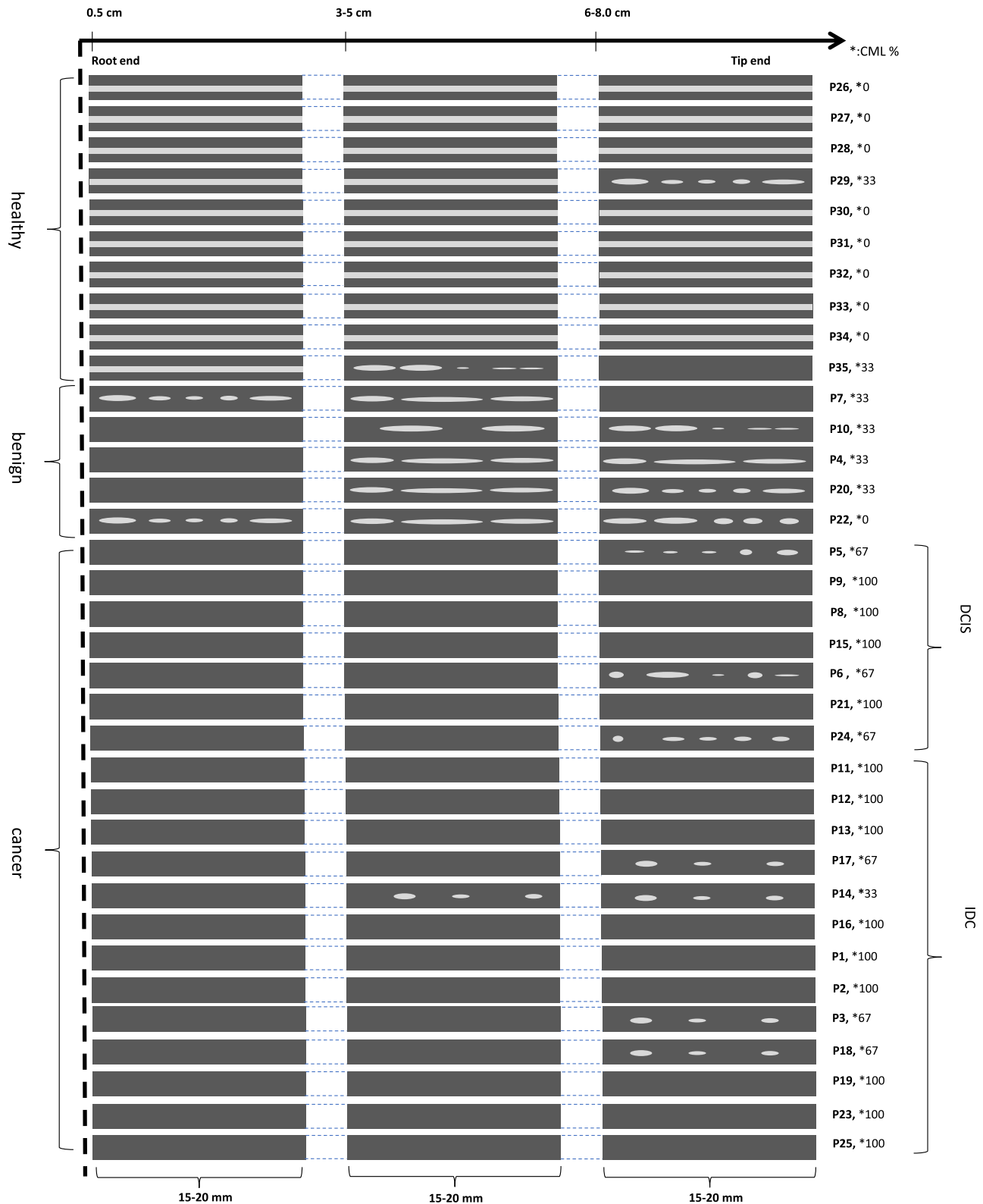

Fig. 6 Schematic diagram of typical medulla structure patterns in hair from cancer, fibroadenoma, and healthy subjects. Note: * describes CML percent in present schematic image of a HS.

and its relative ratio to the NIR wavelength is also very small, resulting in a minimal scattering effect on the cortex from NIR light. However, strong scattering from the medulla suggested the existence of medulla vacuoles (pore-like structures) with a size of 100 nm, close to 0.1 of 860 nm, where maximum scattering is expected.[16] In fact, the medulla showed complex features of vacuoles with variable sizes (0.1 to 4 μm) that were mixed with cortical fibers in an electron microscopy study.[10,17] However, particles such as melanin granules in the cortex closest to the cuticle whose size is 800 nm × 2 μm may reflect or refract light in AOI-dependent manner as shown in Fig 1, resulting in a contribution to light scattering in the dark-field mode of this experiment.[16]

On NIR microscopy, the field of view (FOV) of each examination as single imaging size over the length of HS was 600 μm to 1 mm, whereas the FOV was 400 or 70 μm in IR or SR nanoscopy, respectively.[1] Therefore, an HS of a greater length can be examined more quickly by NIR microscopy than by SR nanoscopy, rendering relatively fast acquisition of imaging patterns in a longer section, more than 2 cm, of a whole HS.

The feature of contrast varied slightly in terms of intensity or thickness of the medulla from individual to individual and between hairs of a given healthy individual. However, the portion of HSs with CML, as shown in Fig. 2(c), was highly increased in cancer patients compared with healthy patients or patients with fibroadenoma. In our previous work,[4] we observed generally that average medulla pattern was continuously distributed along 1.5 to 2 cm of HS in each patient using fast scanning with transmission-type IR microscopy, enabling design of 1.5 to 2 cm as imaging segment unit. In each segment of HS, almost 20 to 30 images could be obtained by NIR microscopy considering 600 μm to 1 mm of FOV. When medulla was either absent or present continuously within more than 90% of the examined unit (1.5 to 2 cm HS), then the dominant pattern was defined as CML or continuous, respectively. All others of the medulla loss distribution were classified as discontinuous (DML or island type) pattern. Dominant pattern of each imaging segment was determined from all integrated 20 to 30 images of each segment of HS and schematically depicted as shown in Figs. 5 and 6.

CML was always observed in all examined cancer patients despite variable frequency among all five samples per patient or the patterns and position of medulla loss along the HS depending on the patient. CML was observed at an average frequency of 85.0 ± 5.6% among all examined samples from each cancer patient. Structural destruction of the hair medulla was also observed in the hair of mice that developed tumors in the

Table 2 Summary of CML extension of cancer HS.

Patient	Age	Diag-coll/day[a]	Histology	Stage	CML to root[b]	CML to tip[b]
P1	45	30	Rt.IDC	T1bN0M0 stage IA	100%	40%
P2	53	33	Rt.IDC	T1bN0M0 stage IA	80%	20%
P3	47	15	Lt.IDC	T1bN0M0 stage IIA	100%	40%
P11	37	16	IDC	T1bN0M0 stage IA	100%	60%
P12	58	13	IDC	T1bN0M0 stage IA	60%	40%
P13	59	30	IDC	T1aN0M0 stage IA	80%	20%
P14	53	24	IDC	T1cN0M0 stage IA	60%	20%
P17	45	61	Lt.IDC	T1bN0M0 stage IIIA	100%	20%
P18	76	114	Rt.IDC	T1bN0M0 stage IIA	100%	40%
P19	42	23	Lt.IDC	T1bN0M0 stage IA	100%	60%
P23	52	40	Rt IDC	T1bN0M0 stage IA	60%	20%
P25	43	29	Rt IDC	T1bN0M0 stage IA	80%	40%
P5	54	11	DCIS	0	80%	40%
P6	47	15	Lt DCIS	0	100%	60%
P8	58	30	DCIS	0	80%	60%
P9	53	0	DCIS	0	80%	60%
P15	78	44	DCIS	0	80%	40%
P21	49	14	Rt.DCIS	0	100%	60%
P24	55	29	Lt. DCIS	0	80%	60%

[a]Time lapse between medical diagnosis (needle biopsy) and hair collection.
[b]Frequency of HS showing CML extension up to root or tip side by 5- to 6-month or 1- to 2-month growth since medical diagnosis, respectively.

mammary gland.[7] Interestingly, HSs from benign fibroadenoma patients demonstrated a typical island-type of pattern in the medulla of all four patients, indicating DML, as shown in Figs. 1(b) and 1(e). However, DML was also observed occasionally in cancer patients, as shown in Fig. 5.

CML was observed in hairs from all cancer patients but at different positions and to different extensions in a whole HS depending on the individual. The position and extension of CML may be related to the time of cancer initiation. Even CML was partly observed in a whole HS from a patient with fibroadenoma, as shown in Fig. 6, but it was relatively short and was always accompanied with DML, compared with the pattern in cancer patients. The average extension of CML per single cancer HS was more than $69.2 \pm 6.5\%$, compared with $33.0 \pm 8.3\%$ in benign HS and $8.5 \pm 3.0\%$ in healthy HS, which may be a helpful diagnostic point for screening breast cancer patients ($p < 0.005$).

Since all hair samples were collected within mostly 2 to 4 weeks after diagnosis by mammography and needle biopsy, the examined part (1.5 to 2 cm) of HS tip side represented hair growth for 1 to 2 months, when considering 1 to 2 cm as average monthly growth rate of hair. Under difficulty in identifying the exact time of cancer initiation with just HS of 10 cm long as grown for 5 to 6 months, we estimated the frequencies of HS showing CML extension up to either the root (5 to 6 months growth since medical diagnosis) or the tip side (1 to 2 months growth near medical diagnosis) from all the examined hair samples ($n = 5$) of each cancer patient and compared DCIS (stage 0) and IDC (stages 1-3) to see the difference in the CML extension. The result was summarized in Table 2. The result showed that the frequency of the CML extending to root side did not show a statistically significant difference between DCIS ($85.7\% \pm 9.7$) and IDC ($85\% \pm 17.3$), and the frequency of the CML extension to tip side was higher in DCIS than in IDC: $54\% \pm 15.1$ versus $35\% \pm 9.8$ ($p < 0.01$). However, the initiation time of tumor development could not be elucidated from this differential distribution of CML. Further study is necessary to investigate the relationship of cancer stage and tumor size with CML distribution. Therefore, it would be important to see the effect of surgical removal of the tumor on the emergence of CML in our future study.

In the past, the medulla was simply regarded as proportional to the diameter of the HS, so thin hair was regarded as hair without medulla. Our data showed no such relationship between the medulla and the diameter of the HS. In contrast, it had some trend that aged hair often showed medulla loss in a discontinuous manner.

4 Conclusions

This study showed feasibility of hair medulla imaging with relatively cheap NIR microscopy by scattering-based contrast between medulla and cortex tissue of hair. The average CML portion of HS in cancer patients was significantly higher than in healthy or benign patients, providing a potential biomarker for screening breast cancer with a relatively cheap imaging setup. It is also an important concern in our future study to investigate the status of CML after surgical removal of a breast cancer tumor.

Disclosures

Authors state no conflicts of interest.

References

1. G. L. Corino et al., "Characterization of a test for invasive breast cancer using x-ray diffraction of hair—results of a clinical trial," *Breast Cancer* **3**, 83–90 (2009).
2. D. A. H. Mistry, J. Haklani, and P. W. French, "Identification of breast cancer-associated lipids in scalp hair," *Breast Cancer* **6**, 113–123 (2012).
3. D. J. Lyman and S. G. Fay, "The effect of breast cancer on the Fourier transform infrared attenuated total reflection spectra of human hair," *Ecancer* **8**, 405–414 (2014).
4. S. M. Han et al., "Synchrotron nanoscopy imaging study of scalp hair in breast cancer patients and healthy individuals: difference in medulla loss and cortical membrane enhancements," *Microsc. Res. Tech.* **79**(1), 23–30 (2016).
5. V. Pecoraro, J. M. Barman, and I. Astore, "The normal trichogram of the adult," *J. Invest. Dermatol.* **44**, 233–236 (1965).
6. R. Saferstein and A. Hall, *Forensic Science Handbook*, 2nd ed., Prentice Hall, New Jersey (2002).
7. V. S. Maryakhina and K. Anenkova, "Change of optical properties of hair cells during malignant tumor development," *J. Biomed. Photonics Eng.* **1**(1), 59–63 (2015).
8. S. Nagase et al., "Influence of internal structures of hair fiber on hair appearance. I. Light scattering from the porous structure of the medulla of human hair," *J. Cosmet. Sci.* **53**(2), 89–100 (2002).
9. S. Nagase, N. Satoh, and K. Nakamura, "Influence of internal structure of hair fiber on hair appearance. II. Consideration of the visual perception mechanism of hair appearance," *J. Cosmet. Sci.* **53**(6), 387–402 (2002).
10. R. Wagner and I. Joekes, "Hair medulla morphology and mechanical properties," *J. Cosmet. Sci.* **58**(4), 359–368 (2007).
11. J. Lim, H. Kim, and S. Y. Park, "Hard x-ray nanotomography beamline 7C XNI at PLS-II," *J. Synchrotron. Radiat.* **21**(Pt. 4), 827–831 (2014).
12. R. K. Curtis and D. R. Tyson, "Birefringence: polarization microscopy as a quantitative technique of human hair analysis," *J. Soc. Cosmet. Chem.* **27**, 411–431 (1976).
13. X. Huang et al., "Review of human hair optical properties in possible relation to melanoma development," *J. Biomed. Opt.* **23**(5), 050901 (2018).
14. A. A. Kharin et al., "Optical properties of the medulla and the cortex of human scalp hair," *J. Biomed. Opt.* **14**(2), 024035 (2009).
15. C. R. Robbins, *Chemical and Physical Behavior of Human Hair*, C. R. Robbins, Ed., p. 92, Springer, Berlin (2012).
16. P. L. Dawson and J. C. Acton, "Impact of proteins on food color," in *Proteins in Food Processing*, R. Y. Yada, Ed., pp. 599–638, Woodhead Publishing, Duxford (2018).
17. R. C. C. Wagner et al., "Electron microscopic observations of human hair medulla," *J. Microsc.* **226**(Pt. 1), 54–63 (2007).

Younshick Choi is an MS student at Daegu Catholic University, School of Medicine, Biomedical Engineering. His current research interests include the integration of NIR microscopy into a mobile device and proton stimulation therapy for Alzheimer's disease.

Young-Ju Jeong is an associate professor and breast surgeon at Daegu Catholic University, School of Medicine. She received her MD and PhD degrees in breast surgery from DCU in 2002 and 2012, respectively. She is the author of more than 50 journal papers and has written three book chapters. Her current research interests include the development of hair-based screening for breast cancer patients.

Jae-Geun Jeon is a PhD candidate at Daegu Catholic University, School of Medicine, Biomedical Engineering. His research involves synchrotron x-ray imaging of hair or biological objects with nanoscale structures, as well as proton therapy for animal models of cancer.

Sung-Hwan Park is a professor of breast surgery at Daegu Catholic University, School of Medicine. He is chairman of the Korean Breast Cancer Society. His research interest is synchrotron imaging of biological specimens.

Hye-Ryeon Choi is a fellow as a breast surgeon at Daegu Catholic University, School of Medicine. She received her MD in breast surgery from the DCU in 2012 and 2017, respectively. Her research interests are synchrotron imaging of biological specimens and investigating biomarkers of breast cancer.

Jong-Ki Kim is currently a professor of biomedical engineering at Daegu Catholic University, School of Medicine. He is a committee member of various professional societies, including Korean Photodynamic Therapy, at the user association of the proton accelerator (KOMAC), the PAL synchrotron facility (KOSUA), and the heavy ion accelerator (RAON). His research interests are therapeutic nanomedicine and proton stimulation therapy for neurodegenerative diseases and brain cancer, as well as the development of high-resolution x-ray transcranial brain imaging techniques.